Structural Chemistry (2019) 30:2123–2133
https://doi.org/10.1007/s11224-019-01330-z

ORIGINAL RESEARCH

Structure-based virtual screening to identify inhibitors against *Staphylococcus aureus* MurD enzyme

Mohammed Afzal Azam[1] · Srikanth Jupudi[1]

Received: 14 February 2019 / Accepted: 27 March 2019 / Published online: 25 April 2019
© Springer Science+Business Media, LLC, part of Springer Nature 2019

Abstract

The MurD enzyme of *Staphylococcus aureus* is an attractive drug target as it is essential and ubiquitous in bacteria but absent in mammalian cells. In the present study, we performed in silico high-throughput virtual screening with small molecule library of 1.60 million compounds to identify potential hits. We used *S. aureus* modeled MurD protein for this purpose and to find the best leads, dock complexes were further subjected to the extra-precision docking and binding free energy calculations by MM-GBSA approach. It is evident that van der Waals and Coulomb energy terms are major favorable contributors while electrostatic solvation energy term strongly disfavors the binding of ligands to the *S. aureus* MurD enzyme. The inhibitory activity of two selected virtual hits **H5** and **H10** was performed against *S. aureus* MurD enzyme using malachite green assay. In in vitro antibacterial screening, compound **H5** inhibited the growth of *S. aureus* NCIM 5021, *S. aureus* NCIM 5022, and methicillin-resistant *S. aureus* (MRSA strain 43300) at high concentrations while the other tested compound **H10** was inactive against all the tested strains. In order to validate the stability of inhibitor-protein complex, compound **H5** with the highest inhibitory against *S. aureus* MurD and lowest binding free energy was subjected to 30-ns molecular dynamics simulation. Further, ADMET predictions showed the favorable pharmacokinetic profile of compounds **H5** and **H10**.

Keywords MurD enzyme · *Staphylococcus aureus* · HTVS · MD simulation · ADMET predictions

Introduction

Infection due to pathogenic bacteria is a leading cause of morbidity and mortality worldwide. The alarming rise of drug-resistant bacteria, such as Gram-positive *Staphylococcus aureus* [1, 2], emphasizes the development of new antibacterial agents for treatment. *S. aureus* is one of the leading causative organisms of infections acquired in the community and after surgery or hospital. It is a human pathogen causing significant morbidity and mortality globally. Apart from skin infections, *S. aureus* is now a major causative organism of bacteremia and infective endocarditis [3, 4] with a negative impact on patient outcomes. This highlights the necessity for developing new antibacterial agents. The intracellular adenosine triphosphate (ATP)-dependent Mur ligase enzymes (MurC-F) are validated as potential therapeutic targets in the antibacterial drug discovery.

The structural integrity of the bacterial cell wall is critically important for the survival of both Gram-positive and Gram-negative bacteria. By maintaining the cell shape and providing rigidity, the bacterial peptidoglycan plays a crucial role in cell survival. This peptidoglycan, comprising sugar molecules and peptides is synthesized and integrated outside the cytoplasmic membrane of the cell. For many years, disruption of the peptidoglycan layer is considered a prime target for the development of effective antibacterial agents. This rigid layer is incorporated by a multi-step synthesis and consists of many targets that do not exist in the human cell. Central to this pathway are four topologically similar ATP-dependent Mur ligases MurC, MurD, MurE, and MurF. These enzymes are involved in the intracellular assembly of peptidoglycan by catalyzing the consecutive addition of L-Ala, D-glutamic acid (D-Glu), meso-diaminopimelic acid (m-DMPA) (or L-Lys), and D-Ala-D-Ala to the starting precursor UDP-N-acetylmuramic acid (UDP-

Electronic supplementary material The online version of this article (https://doi.org/10.1007/s11224-019-01330-z) contains supplementary material, which is available to authorized users.

✉ Mohammed Afzal Azam
afzal9azam@hotmail.com; afzal@jssuni.edu.in

[1] Department of Pharmaceutical Chemistry, JSS College of Pharmacy, Ooty, Tamil Nadu 643001, India

MurNAc) [5, 6]. The Mur ligases operate by a common reaction mechanism [7] and share similar three-dimensional structures with conserved amino acid regions [8–10]. They are functionally essential for the survival of bacteria. Further, the ATP-dependent catalytic pocket of the Mur ligases shows the highest level of sequence and structural similarity [8] but they are not closely related to any ATP-utilizing human enzyme [11]. MurD is second in the series of Mur ligases that catalyzes the formation of a peptide bond between D-Glu and cytoplasmic intermediate uridine-5′-diphosphate-N-acetylmueamoyl-L-alanine (UMA). Due to its high specificity for the D-amino acid substrate, involvement in the synthesis of peptidoglycan, and its absence in mammals, MurD enzyme is considered as an attractive target for the development of new antibacterial agents [12, 13]. Further, the cloned MurD from *S. aureus* showed high percentage similarity to MurD proteins from *Streptococcus pyogenes* (66%), *Bacillus subtilis* (65%), *Escherichia coli* (54%), and *Haemophilus influenzae* (55%) [14].

The catalytic pocket of MurD comprises an N-terminal domain, a central domain, and a C-terminal domain. The N-terminal domain comprises five-stranded parallel β-sheet surrounded by four helices [15, 16] and is mainly involved in the specific recognition of the nucleotide substrate. This domain binds the nucleotide substrate UDP moiety through a cleft constituted by the diphosphate-binding pocket and two hydrophobic loops. The central binding domain consists of six-stranded parallel β-sheet which is surrounded by seven α-helices and flanked on both sides by smaller antiparallel three-stranded β-sheet. These parallel β-sheets play an important role in the binding of adenosine triphosphate (ATP). The C-terminal domain consists of six-stranded β-sheet (five parallel and one antiparallel β-strands) and is surrounded on both sides by five α-helices. This domain also called as Rossmann fold is primarily responsible for the binding of substrates amino acid or dipeptide [6, 17]. The ATP-binding pocket of MurD enzyme is present in a cleft formed between the central and C-terminal domains. In addition to loop, the C- and N-terminal binding domains also undergo conformational changes when the substrate binds with the enzyme. The MurD bring together the UMA and ATP in the cleft and orient them properly in the catalytic pocket for the formation of an acylphosphate intermediate. At the binding site, MurD also orients the D-glutamine for the nucleophilic attack and thereby stabilizes the tetrahedral intermediate [18]. Further, site-directed mutagenesis indicated that among different bacterial Mur ligases, the GXXGKT/S ATP-binding consensus sequence and seven residues are common invariants [19]. However, differences exist in the overall topologies and amino acid sequences of MurD binding pockets from *S. aureus*, *E. coli, Mycobacterium tuberculosis*, *Streptococcus pneumonia*, and *Borrelia burgdorferi*. *S. aureus* MurD showed a high degree of sequence similarity with *S. pneumonia* MurD but low sequence similarity was observed with MurD from *B. burgdorferi*, *E. coli*, and *M. Tuberculosis* [20].

Novel phosphinates, phosphonates, and N-acetylmuramic acid analogs have been developed as transition-state analog inhibitors of *E. coli* MurD; however, these compounds did not show promising results [21–24]. Phosphorylated hydroxyethylamines have been reported to have inhibitory activity against the whole MurC to MurF cascade [25] with IC_{50} values in the micromolar range. This paved the way for the development of multiple inhibitors of Mur ligases. In a further development, substituted naphthalene-N-sulfonyl derivatives of glutamic and substituted analogs of D-glutamic acid have been synthesized and evaluated as a potential inhibitor of the MurD from *E. coli* [26–29]. Further, it has been shown that L-Glu-containing compounds can also inhibit MurD ligase, despite the intrinsic preference for the D-Glu amino acid by MurD [26, 27]. 5-Benzylidenerhodanine and 5-benzylidenethiazolidine-2,4-dione-based *E. coli* MurD inhibitors were designed and synthesized. High-resolution 3D crystal structures of these D-Glu-based inhibitors [30, 31] provided insight into the molecular basis for binding within the catalytic pocket. In further development, naphthalene-N-sulfonyl derivatives possessing conformationally rigidified mimetics of D-Glu have been synthesized and evaluated as inhibitors of *E. coli* MurD [32, 33]. Some of these rigid mimetics displayed promising inhibitory activity against the whole cascade of Mur ligases (MurD-MurF). Structure-based virtual screenings and target-based design approach have been employed to identify novel MurD inhibitors [34–36]. But these efforts not resulted in inhibitors with potent antibacterial activity. Further, based on the virtual screening result and de novo structure-based design, *E. coli* MurD D-Glu-based inhibitors possessing 5-benzylidenethiazolidin-4-one scaffold are reported with improved potency (IC_{50} between 3 and 7 μM) [37]. However, only a few of these compounds exhibited weak activity against *S. aureus* and *Enterococcus faecalis*. Further, 2-thioxothiazolidin-4-one-based inhibitors with IC_{50} in the micromolar range against *S. aureus* MurD enzyme is reported [38]. One of these compounds exhibited significant inhibitory activity against methicillin-resistant *S. aureus* (MRSA) ATCC 43300 and *S. aureus* ATCC 29213 with MIC values of 8 μg/mL.

The aim of the present study was to identify potential virtual hits with inhibitory potency against *S. aureus* MurD ligase. The homolog 3D structure of *S. aureus* MurD prepared earlier [39] was used for the present study. Using structure-based in silico high-throughput virtual screening (HTVS) approach, potential hits were identified from library databases of approximately 1.6 million compounds. A filter based on docking energy identified ten potential hits with high negative binding free energy against the modeled *S. aureus* MurD ligase. The binding mode and stability of one of the hit and

protein complex were analyzed by molecular dynamics (MD) simulation.

Materials and methods

In silico high-throughput virtual screening

We carried out structure-based high-throughput virtual screening using the Glide docking module incorporated in Schrödinger, LLC, New York, 2018-1. Earlier prepared homolog 3D structure of *S. aureus* MurD was employed as 3D search query using the available library databases (Enamine, lifeChemicals, TimTec, Asinex, Specs, ChemDiv, KeyOrganics, Maybridge) of approximately 1.60 million compounds. Molecules with high binding affinity within the catalytic pocket of *S. aureus* MurD were captured as hits and ranked according to their standard precision docking score. A total of top 3820 ligands ranked by the HTVS were clustered using normalized volume overlap with a grid spacing of 1.0 Å option into ten groups each inhabiting a different chemical space. Forty molecules from each cluster with the highest docking score were selected and subjected to Glide standard precision (SP) docking. Top 10% of molecules were analyzed to discard compounds with lower Glide score and not forming hydrogen bonding and hydrophobic interactions in the catalytic pocket. The selected 40 virtual hits were further docked into the catalytic pocket of modeled *S. aureus* MurD protein in an extra-precision mode using energetic-based Glide [40] without applying any constraints. Ten virtual hits **H1**–**H10** were selected based on Glide score, Glide model energy, Glide energy, and hydrogen bond interactions (Table 1, Supplementary Fig. S1, and Table S1). Subsequently, their binding free energies were calculated using the Prime Molecular Mechanics Generalized Born Surface Area (MM-GBSA) method [41] (Table 2) with an OPLS3 force field and VSGB 2.0 energy model [42]. Molecular docking and binding free energy calculation were carried out using protocols described earlier [39]. Notably, the identified hits **H1**–**H10** had scaffold topology different from earlier reported inhibitors of MurD. Additionally, Qikprop simulation was performed on all ten identified compounds to characterize the absorption, distribution, metabolism, excretion, and toxicity (ADMET) properties of all compounds (Supplementary Table S2). Further, the docked complexes of virtual hit **H5** with modeled *S. aureus* MurD were used to run 30 ns molecular dynamics simulation.

Molecular dynamics

In order to validate the stability and to get insight into the binding modes of virtual hit **H5** within the catalytic pocket of modeled *S. aureus* MurD, 30 ns MD simulations were performed using the Desmond [43] software with OPLS3 force field [44]. The docked complex **H5**/*S. aureus* MurD protein was solvated with the TIP4P solvent model [45, 46] in an orthorhombic box keeping a 10 Å buffer region between protein atoms and box sides. Overlapping water molecules were deleted and then the system was neutralized by adding 10 sodium ions. The solvated system contains 47,571 atoms (including 13,478 water molecules) and 1,122,523 $Å^3$ final box volume. Limited-memory Broyden Fletcher Goldfarb Shanno (LBFGS) minimization of the whole system was carried out with a minimum of 10 steepest descent steps, 3 vectors, and a gradient threshold of 25 kcal/mol/Å. During minimization, the maximum iterations were 2000 with a convergence threshold of 1.0 kcal/mol/Å. The system was then gradually heated to 300° K in the NPT ensemble with a time step of 2 fs. A multiple time step reversible reference system propagator algorithms (RESPA) integration algorithm was employed throughout the MD simulation with time steps of 2 fs for bonded, 2 fs for near nonbonded, and 6 fs for far nonbonded interactions. The particle mesh Ewald (PME) method [47] was employed for computing the long-range electrostatic interactions with a 9 Å short-range cutoff radius for van der Waals and Coulomb interactions. The system was then subjected to a 30 ns MD simulation in the NPT ensemble (T = 300 K, thermostat relaxation time = 200 ps; p = 1 atm; barostat relaxation time = 200 ps) using a Nose–Hoover thermostat [48] and Martyna–Tobias–Klein barostat [49]. The MD trajectory and 3D structures were visually inspected and analyzed using the Maestro graphical interface. The results of root mean square deviation (RMSD), root mean squared fluctuation (RMSF), and interactions of **H5** with the catalytic pocket residues have been incorporated into the results.

S. aureus MurD activity inhibition assay

High-throughput virtual hits **H5** (Enamine T1827917) and **H10** (Enamine T1990672) were procured from Enamine Ltd., Kiev, Ukraine. The inhibitory activity of these two selected compounds was determined against *S. aureus* MurD (ProFoldin, USA) as described earlier [50, 51] by the malachite green assay with slight modifications. All of the experiments were run in duplicate. The assay mixture with final volume of 50 μL consisted of the following: 500 mM TrisHCl, pH 8.0, 400 mM KCl, 10 mM DTT, 0.05% Triton X-100, 10 mM $MgCl_2$, 1 mM UDP-MurNAc-L-Ala, 5 mM D-Glu, 10 mM ATP, 5000 nM purified MurD from *S. aureus*, and 0.6 μL of different concentrations of each tested compound dissolved in DMSO. In all cases, the final concentration of DMSO was 5% (*v*/*v*). The reaction was initiated by the addition of MurD enzyme to the assay mixture and was incubated at 37 °C for 60 min and then quenched with Dye MPA3000. Incubated for 5 min and absorbance was measured at 650 nm and percentage inhibition of each compound was calculated with respect to a negative control (0% activity) and

Table 1 Extra-precision docking score of selected virtual hits **H1**–**H10** in the active site of modeled *S. aureus* MurD ligase (kcal/mol)

Virtual hits	Molecule code	[a]G_{score}	[b]G_{vdw}	[c]G_{Coul}	[d]G_{emodel}	[e]G_{energy}	[f]G_{Lipo}
H1	Asinex BAS 00394574/CACPD2011a-0000133428	− 9.77	− 46.78	− 11.41	− 82.17	− 58.19	− 4.34
H2	Specs AN-465/42162586/CACPD2011a-0001430246	− 9.04	− 57.02	− 6.99	− 85.19	− 64.01	− 4.12
H3	Enamine T0517-1728/CACPD2011a-0001561858	− 8.06	− 54.84	− 7.77	− 89.92	− 62.61	− 5.33
H4	Enamine T6670231/CACPD2011a-0002274684	− 9.02	− 45.42	− 10.18	− 76.9	− 55.60	− 3.83
H5	Enamine T6806127/CACPD2011a-0001827917	− 10.23	− 44.03	− 18.66	− 93.53	− 62.69	− 6.33
H6	Enamine T0509-0136/CACPD2011a-0001428266	− 9.83	− 46.11	− 9.32	− 73.83	− 55.44	− 3.83
H7	Asinex BAS 01362697/CACPD2011a-0001561840	− 9.60	− 51.71	− 5.03	− 78.83	− 56.74	− 4.34
H8	Enamine T5632111/CACPD2011a-0001995256	− 9.03	− 46.47	− 2.28	− 66.03	− 48.75	− 3.99
H9	Enamine T5354241/CACPD2011a-0000848041	− 9.11	− 56.22	− 10.79	− 108.97	− 67.01	− 5.55
H10	T0500-2187/CACPD2011a-0001990672	− 9.88	− 57.73	− 7.91	− 104.34	− 65.65	− 5.36

[a] Glide score

[b] Glide van der Waals energy

[c] Glide Coulomb energy

[d] Glide model energy

[e] Glide energy

[f] Glide lipophilic contact plus phobic attractive term in the glide score

enzyme reaction (100% activity). IC_{50} values were determined using the GraphPad PRISM.

Antibacterial activity

The antibacterial activity of two selected virtual hits **H5** (Enamine T1827917) and **H10** (Enamine T1990672) was carried out against Gram-positive *S. aureus* (NCIM 5021 and NCIM 5022), methicillin-resistant *S. aureus* (MRSA strain 43,300), and *B. subtilis* (NCIM 2545), and Gram-negative strains *E. coli* (NCIM 2567), *K. pneumonia* (NCIM 2706), and *P. aeruginosa* (NCIM 2036) according to the guidelines of the Clinical Laboratories Standard Institute [52]. Triplicate analyses were performed for each of the selected strains. Microdilution broth technique was employed to determine MIC values by using the Mueller Hinton medium (Hi-media). Test compounds were dissolved in sterile dimethyl sulfoxide (DMSO) and sterile DMSO was used as a negative control. Ciprofloxacin and methicillin were used as control drugs (positive) in sterile DMSO. Plates were incubated at 37 °C for 24 h and were read for the MIC (Fig. 1).

Results and discussion

Extra-precision docking and binding free energy by prime MM-GBSA

Analysis of the extra-precision docking poses of virtual hits **H1**–**H10** exposed hydrogen bonding, π-π stacking, and salt bridge interactions mainly in the region of Lys19 to Gly147 and Lys328-Gln432 (Fig. 2 also Supplementary Fig. S1 and Table S1). A comparison of different docking poses of **H1**–**H10** exhibited interactions with Lys19, Gly80, Glu101, Ser168, His196, Arg355, Trp425, Asp426, and Gln432 (Supplementary Table S1) residues belonging to the amino acid stretch that forms the catalytic pocket. Glide score of compounds **H1**–**H10** ranges from − 10.23 to − 9.02 kcal/mol (Table 1); the highest glide score of − 10.23 kcal/mol was observed with **H5**. To illustrate the binding mode, compounds **H1**, **H5**, and **H10** were analyzed and results were compared. As shown in the docked pose of **H1** (Fig. 2a) in the active site of *S. aureus* MurD, the NH of one of the protonated piperidine ring formed hydrogen bonding interaction with the side chain carbonyl oxygen of Asp426 ((>N^+(H)H···O=C<, 2.18 Å). The nitrogen of the same ring established a salt bridged interaction with the carboxylate oxygen of Asp426. The carbonyl oxygen and NH adjacent to this piperidine ring exhibited hydrogen bonding interactions respectively with the backbone NH of Trp425 (>C=O···NH, 2.50 Å) and backbone NH of Pro79 (NH···O=C<, 1.96 Å). The other carbonyl oxygen of this compound formed two hydrogen bonding interactions one each, respectively with the side chain protonated ring nitrogen of His196 (>C=O···rNH^+, 1.82 Å) and the side chain NH of Arg355 (>C=O···NH, 2.05 Å). The docked pose of compound **H5** exhibited seven hydrogen bonds (Fig. 2b), two more than compound **H1**. Precisely, OH group present on one of the terminal phenyl ring accepted a hydrogen bond from the side chain carboxylate oxygen of Glu23 (OH···$^-$O–C=O, 1.84 Å). The two NH of –NHCONH– fragment adjacent to this hydroxyphenyl ring formed one hydrogen bonds each with the backbone NH of Gly147, while the carbonyl oxygen of the same fragment exhibited hydrogen bonding interaction with the side chain NH of protonated Lys19

Table 2 Binding free energy contribution (MM-GBSA) of selected virtual hits **H1**–**H10** in the active site of modeled *S. aureus* MurD ligase (kcal/mol)

Comp.	[a]ΔG_{Coul}	[b]ΔG_{Solv}	[c]ΔG_{Lipo}	[d]ΔG_{vdW}	[e]$\Delta G_{H\text{-}bond}$	[f]ΔG_{cov}	[g]$\Delta_{packing}$	[h]ΔG_{Bind}
H1	− 47.77	14.85	− 22.15	− 40.21	− 4.42	− 12.34	− 1.73	− 82.79
H2	− 59.74	60.11	− 20.41	− 81.41	− 7.65	12.87	− 2.3	− 83.00
H3	− 41.39	60.28	− 27.28	− 69.06	− 3.2	2.11	− 3.64	− 77.98
H4	− 31.29	35.95	− 15.66	− 48.71	− 3.35	1.93	− 1.34	− 74.84
H5	− 82.75	41.93	− 15.53	− 35.71	− 7.88	32.29	− 1.02	− 88.89
H6	− 43.56	39.39	− 18.54	− 35.77	− 0.92	0.43	− 1.96	− 66.16
H7	− 43.52	35.56	− 10.3	− 26.85	− 0.04	− 20.94	− 4.85	− 66.14
H8	− 73.12	36.41	− 24.83	− 46.69	− 7.18	33.39	− 6.28	− 66.12
H9	− 76.37	67.31	− 24.13	− 61.21	− 6.66	8.13	− 1.85	− 65.03
H10	− 36.42	57.24	− 20.56	− 39.72	− 5.25	− 28.39	− 1.72	− 86.50

[a] Coulomb energy

[b] Electrostatic solvation energy

[c] Hydrophobic energy (non-polar contribution estimated by solvent-accessible surface area)

[d] van der Waals energy

[e] Hydrogen-bonding energy

[f] Covalent binding energy (internal energy)

[g] π-π packing energy

[h] Free energy of binding

(>C=O···$HN(H_2)^+$). Additionally, this hydroxyphenyl ring also exhibited two π-π stackings, one each with the pyrrole and benzo parts of the Trp425. This lucrative hydrophobic interactions further stabilized compound **H5** in the catalytic pocket. The central phenyl ring showed a π-cation interaction with the protonated nitrogen of Lys19 while the OH present on another terminal hydroxyphenyl ring established two hydrogen bonding interactions one each with the backbone NH of Gly80 (HO···NH, 2.04 Å) and the side chain carboxylate oxygen of Glu101 (OH···$^{-}$O–C=O, 1.71 Å). It is evident that all of the hydrogen bonding interactions for this compound is in the N-terminal and central domain of the catalytic pocket. On the other hand, docking pose of compound **H10** (Fig. 2c) showed four hydrogen bonding interactions, three less compared to compound **H5**. Hydrogen bonding interaction for this compound was observed with Lys19, Ser168, Ala423, and Gln432, key binding residues of catalytic pocket. Our extra-precision docking result also exposed a π-π stacking interaction of one of the phenyl ring with the phenyl ring of Phe170. However, no π-cation interaction was observed for this compound. It is evident that compound **H10** occupied all three domains of the catalytic pocket and established hydrogen bonding interactions with residues of all three domains. Further, generated binding cavity pocket (Supplementary Fig. S2) showed that the compound **H5** is well placed within the catalytic pocket and both –NH–CO–NH– fragments are oriented towards hydrogen bond acceptor regions (red color).

Prime MM-GBSA-based binding free energy was calculated for rank ordering of the poses of virtual hits **H1**–**H10**. The calculated free energies of binding (ΔG_{bind}) ranges from − 88.89 to 65.03 kcal/mol indicating the high binding affinity of compounds **H1**–**H10** within the catalytic pocket of modeled *S. aureus* MurD enzyme. It is evident from Table 2 that the van der Waals ($\Delta G_{vdW,}$ − 82.75 to − 31.29 kcal/mol) and Coulomb (ΔG_{Coul}, 26.85 to 81.41 kcal/mol) energy terms are major favorable contributors for ligands binding. The electrostatic solvation energy (ΔG_{Solv}, 14.85 to 67.31 kcal/mol) term strongly disfavors the binding, whereas non-polar contribution (ΔG_{Lipo}) interactions moderately favor the binding of all compounds. Covalent binding energy moderately favors the binding of compounds **H1** and **H7**, whereas it disfavors the binding of all other compounds. Moreover, high negative values of ΔG_{Coul} indicated that the catalytic pocket is lined with the polar residues and there is less contribution from the hydrophobic residues for ligands binding to the modeled *S. aureus* MurD enzyme. It is also evident from the high negative values of ΔG_{vdW} that ligands are buried well within the polar region upon binding and this is in agreement with our docking result (Table 1) where van der Waals interaction energy also favors the ligands binding.

The identified virtual hits **H1**–**H10** obeyed Lipinski's rule of five (0 to 2), indicating the drug like property of these molecules (Supplementary Table S2). These molecules are devoid of CNS activity as indicated by the predicted central nervous system (CNS) activity (− 2 to 1) on a scale of − 2 as inactive and + 2 as active. The polar surface area (PSA) which is indicative of van der Waals surface area of polar nitrogen and oxygen atoms of molecules ranges between 76.98 to

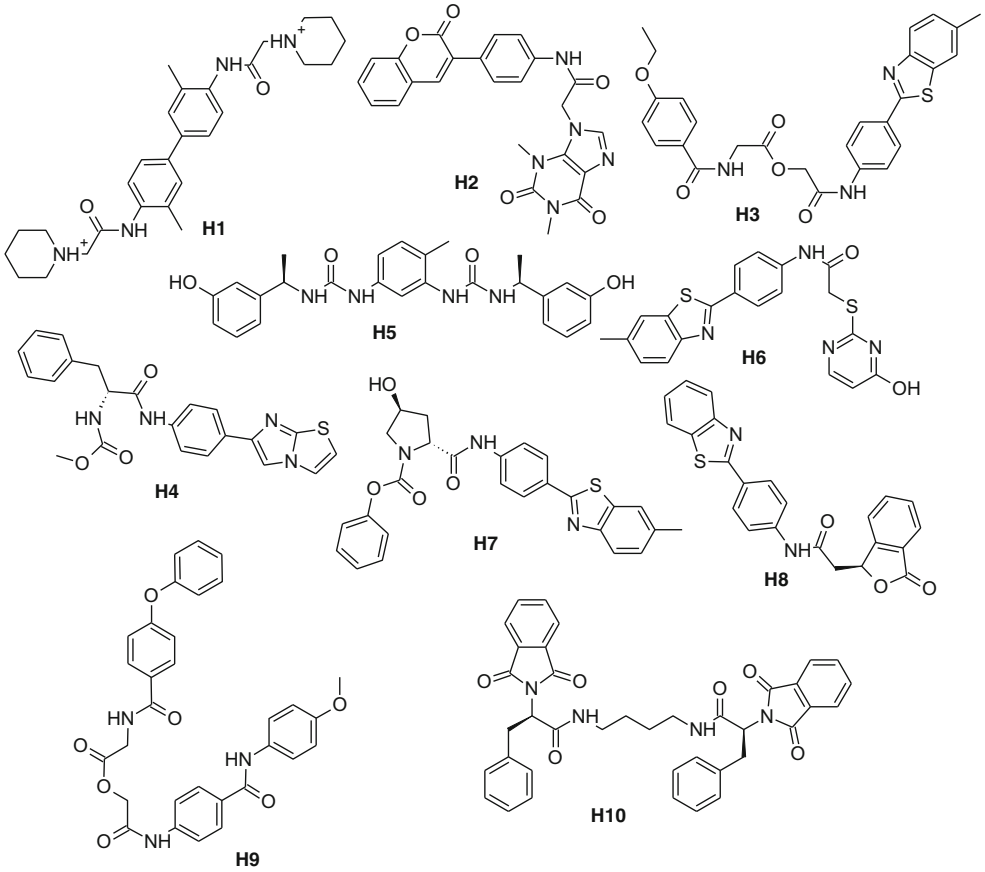

Fig. 1 Represents chemical structures of potential hits **H1**–**H10** obtained by structure-based high-throughput virtual screening

172.52 Å^2 and is well within the recommended range of 7–200 A^2. QPlogPo/w which is related to the hydrophobicity of the molecule is in the range of 2.19 to 5.22 and is well within the recommended range of—2.0 to 6.5. The predicted apparent Caco-2 cell permeability which is a model for the gut-blood barrier is the range 60.79 to 1023 nm/s, indicating non-active transport of these molecules. Predicted human oral absorption of **H1**–**H10** is in the range of 71.71 to 100% on a scale of 0 to 100%. For virtual hits **H5** and **H10**, the predicted IC_{50} values for the blockage of human ether-a-go-go (HERG) K^+ channels (QPlogHERG) are − 4.76 and − 4.58, respectively indicating the safety of these molecules. While QPlogHERG values for other eight compounds (**H1-H4** and **H6-H9**) range between − 6.55 to − 9.02, indicating the blockage of HERG K^+ channels and hence probable cardiac toxicity of these molecules. Further, lower solvent accessible surface area (SASA) of these molecules (688.42 to 973.40 Å^2) on a recommended range of 300–1000 Å^2 indicated the burial of these molecules within the catalytic pocket.

S. aureus MurD activity inhibition assay

Based on the extra-precision docking and MM-GBSA results, two best-ranked virtual hits **H5** (Enamine T1827917) and **H10** (Enamine T1990672) were tested against *S. aureus* MurD in the malachite green assay [50, 51]. The IC_{50} values were determined for both compounds, and in both cases, they were in the micromolar range. The most active compound, **H5** (Enamine T1990672), has an IC_{50} of 7 μM whereas compound **H10** showed an IC_{50} of 30 μM. The two active compounds **H5** and **H10** arising from the molecular docking analysis were among the first 10 top-ranked database compounds identified.

Antibacterial activity

The antibacterial activity of the hit compounds **H5** (Enamine T1827917) and **H10** (Enamine T1990672) was determined against Gram-positive *S. aureus* (NCIM 5021 and NCIM 5022), methicillin-resistant *S. aureus* (MRSA strain 43,300), *B. subtilis* (NCIM 2545), and Gram-negative strains *E. coli* (NCIM 2567), *K. pneumonia* (NCIM 2706), and *P. aeruginosa* (NCIM 2036) (Table 3). None of the tested hit compounds demonstrated antibacterial activity against *E. coli* (NCIM 2567), *K. pneumonia* (NCIM 2706), *P. aeruginosa* (NCIM 2036), and *Bacillus subtilis* (NCIM 2545). Compound **H10** was also observed to be inactive against *S. aureus* (NCIM 5021 and NCIM 5022), methicillin-resistant *S. aureus* (MRSA strain 43,300), and *B. subtilis* (NCIM 2545) while compound **H5** prevented growth of

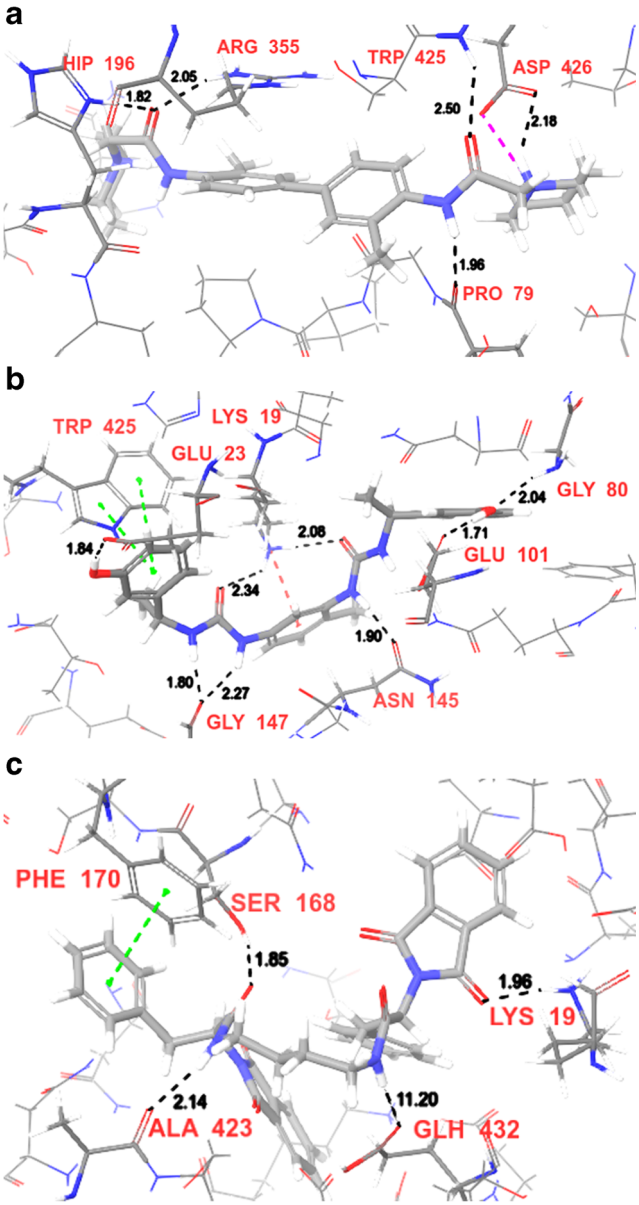

Fig. 2 Represent the interactions of virtual hits (**a**) **H1**, (**b**) **H5**, and (**c**) **H10** with the catalytic pocket residues of modeled *S. aureus* MurD ligase

S. aureus NCIM 5021, *S. aureus* NCIM 5022, and methicillin-resistant *S. aureus* (MRSA strain 43,300) at higher concentrations (MIC 128, 128, and 256 μg/mL, respectively). The lack of antibacterial activity is probably due to the failure of these compounds to enter the bacterial cell.

Minimum inhibitory concentration

Molecular dynamics

The MD simulation of the docked **H5**/modeled *S. aureus* MurD complex was performed to get insight into the mechanistic aspects of the protein-ligand interactions. The trajectory frames obtained from the simulation were inspected to analyze the predicted binding pose of **H5**. The RMSD values of protein all backbone, C-α, and heavy atoms in the inhibitor/modeled protein complex increased to 4.41, 4.34, and 4.59 Å, respectively during equilibration phase of 15 ns (Fig. 3a). After the equilibration phase, the mean RMSD values of complex backbone, C-α, and heavy atoms were observed to be 0.51, 0.475, and 0.65 Å, respectively during 15 to 30 ns MD trajectory. This indicated that there are no significant structural changes in protein during simulation. It is also evident from Fig. 3 a that the binding pocket residues RMSD cope well with the ligand movement. The radius of gyration (rGyr) of both backbone (blue circle) and C-α (red triangle) atoms throughout the MD trajectory is shown in Supplementary Fig. S3. The rGyr of backbone (blue circle) and C-α (red triangle) atoms gradually increased up to 15 ns and then stabilized respectively in the range 3.24 to 4.54 and 3.12 to 4.51 Å, during rest of the simulation time. This further indicated that the whole system is in relaxed conformations resulted from solvent effect. Further, protein all backbone and C-α atoms of catalytic pocket binding residues exhibited the RMSF values in the range 0.87–2.43 Å and 0.85–2.40, respectively (Fig. 3b) indicating low fluctuations of these residues. The high fluctuations of backbone and C-α atoms RMSF were observed between amino acid stretches Leu43-Gln45 (2.70–3.24 and 2.52–3.34 Å, respectively) present on loop (Asp39-Ala47) and Ser341-Gln344 (3.30–3.68 and 3.32–3.3.78 Å, respectively) present on β-sheet (Ile346-Gly351). These residues are away from the catalytic pocket.

Among eight hydrogen bonds predicted in XP-docking simulation, seven hydrogen bonds were preserved for compound **H5**/*S. aureus* MurD complex during 30 ns MD simulation. It is evident from Fig. 3 c and d (also Supplementary Fig. S4) that compound **H5** occupied mainly N-terminal and central domains of modeled MurD catalytic pocket. The binding of **H5** within the catalytic pocket was observed to be driven by both hydrogen bond and hydrophobic interactions with the conserved residues Lys19, Glu23, Gly80, Glu101, and Gly147. It is also evident that both hydroxyphenyl rings and –NH–CO–NH– fragments are responsible for the recognition of this compound within the active site. Both hydroxyphenyl rings are positioned at the UDP-MurNAc-L-Ala-D-Glu (UMAG) site, the binding site of a D-Glu moiety of other MurD inhibitors containing the D-Glu moiety [37, 53] while urea moieties occupied both UMAG and ATP binding sites.

Accurately, OH present on one of the phenyl ring formed a water-mediated high-frequency hydrogen bond (75% of the MD trajectory) with the side chain carboxylate oxygen of Glu23 (OH$\cdots^{-}$O–C=O). This high-frequency interaction is evolved due to the less conformational flexibility of Glu residue ($\psi = 30°$) (Supplementary Fig. S5a). This phenyl ring also exhibited a high-frequency π-cation interaction (74% of the MD trajectory) with the side chain NH of protonated

Table 3 Antibacterial activity of synthesized compounds **4a-s** and **9a-f** against Gram-positive and Gram-negative bacteria

Comp.	Minimum inhibitory concentration (μg/mL)*						
	[a]*S. a*	[b]*S. a*	[c]*S. a*	[d]*B. s*	[e]*K. p*	[f]*P. a*	[g]*E. c*
H5	128	128	256	128	> 256	> 256	> 256
H10	> 256	> 256	> 256	> 256	> 256	> 256	> 256
Ciprofloxacin	2	2	32	2	2	2	2
Methicillin	4	4	16	8	–	–	–

*Average of three independent determinations

[a] *S. a*, *Staphylococcus aureus* NCIM 5021

[b] *S. a*, *Staphylococcus aureus NCIM 5022*

[c] *S. a*, *Staphylococcus aureus* ATCC 43300 (MRSA)

[d] *B. s*, *Bacillus subtilis* NCIM 2545

[e] *K. p*, *Klebsiella pneumoniae* NCIM 2706

[f] *P. a*, *Pseudomonas aeruginosa* NCIM 2036

[g] *E. c*, *Escherichia coli* NCIM 2567

Lys19 and a low-frequency π-π stacking (26% of the MD trajectory) with the side chain phenyl ring of Trp425. The high-frequency interaction is due to the less conformational flexibility of Lys 19 (ψ = 30°, Supplementary Fig. S5b) whereas the low-frequency π-π stacking interaction is evolved due to high conformational flexibility of Trp425 (ψ = 120°, Supplementary Fig. S5c). Both NH of –NH–CO–NH– fragment attached to this phenyl ring exhibited strong hydrogen bonding interactions (86% of the MD trajectory in both cases) with the backbone carboxylate oxygen of Gly147 (NH···O=C<) in a bidentate manner. It is evident from supplementary Fig. S5d that this strong hydrogen bonding interaction is probably due to the less conformational flexibility of Gly147 residue (ψ = 35°) during most of the simulation time. The carboxylate oxygen of the same fragment accepted a high-frequency hydrogen bond (56% of the MD trajectory) from the side chain NH of Lys19 (>C=O···$HN(H_2)^+$). The oxygen of OH group present on another phenyl ring exhibited a strong frequency hydrogen bonding interaction with the backbone NH of Gly80 (HO···NH, 65% of the MD trajectory), while the hydrogen of same OH group formed a water-mediated low-frequency (27% of the MD trajectory) hydrogen bond with the side chain carboxylate oxygen of Glu101 (OH···$^-$O–C=O). This low-frequency interaction is probably due to the high conformational flexibility of Glu101 residue throughout the 30-ns simulation. The carbonyl oxygen of –NH–CO–NH– function attached to this another phenyl ring exhibited a high frequency (54% of the MD trajectory) direct hydrogen bonding interaction (>C=O···$HN(H_2)^+$) and a water-mediated moderate frequency (34% of the MD trajectory) hydrogen bonding interaction with NH of Lys19 (>C=O···H(H)O···$HN(H_2)^+$).

During MD simulation, the rGyr of the ligand was in the range 5.07 to 5.57 Å, which indicates the ligand stability within the catalytic pocket (Supplementary Fig. S6). The lower RMSD value in the range of 0.89 to 1.96 Å further shows the less conformational flexibility and stability of ligand during MD simulation. The solvent accessible surface area (SASA) of ligand **H5** was observed to be stable in the range 135.44 to 238.62 $Å^2$ throughout the 30-ns simulation time indicating no significant change in the binding pocket volume. The polar surface area (PSA) of **H5** was observed to in the range 189.80 to 215.32 $Å^2$ during the last 25 ns of MD simulation, indicating the complete burial of compound within the hydrophilic pocket and this is in agreement with the docking study result (Supplementary Fig. S2). The generated simulation quality analysis result (Supplementary Fig. S7) of **H5**/*S. aureus* complex showed the total energy of the system between − 125,600 to − 125,200 kcal/mol, further indicating the stability of the modeled protein during 30-ns MD simulation. Further, superposition of the conformations of **H5** after MD simulation and best XP-docked pose exhibited similar orientation with a low RMSD value 0.821 Å (Supplementary Fig. S8), indicating the conformational stability of binding pocket and ligand **H5** during MD simulation. Above obtained results also indicated the rationality and validity of docking protocols used.

Conclusion

The murD enzyme is second in the series of Mur ligases and plays an important role in the formation of a peptide bond between D-Glu and cytoplasmic intermediate UMA. Its high specificity for D-amino acid substrate and its absence in mammals makes MurD a promising target for the development of new antibacterial agents. In the present study, we performed structure based in silico high-throughput virtual screening against *S. aureus* MurD enzyme using a compound library of ~ 1.6 million small molecular entities. Ten virtual hits **H1**–**H10** was selected based on the extra-precision Glide score, interactions within the catalytic pocket, and high negative values of binding free energy. Binding free energy calculation by MM-GBSA approach showed van der Waals and Coulomb energy terms as major favorable contributors for ligand binding. While electrostatic solvation energy term, strongly disfavors the binding of ligands to the *S. aureus* MurD enzyme. Among the ten selected compounds, two compounds **H5** and **H10** showed favorable ADMET profile with low affinity for HERG K^+ channels. The inhibitory activity of these two compounds against *S. aureus* MurD enzyme was performed using the malachite green assay. Compound **H5** exhibited the highest activity with IC_{50} values of 7 μM while compound **H10** displayed lower activity with an IC_{50} value of 30 μM. Compound **H5** inhibited the growth of *S. aureus* NCIM 5021, *S. aureus* NCIM 5022, and methicillin-resistant

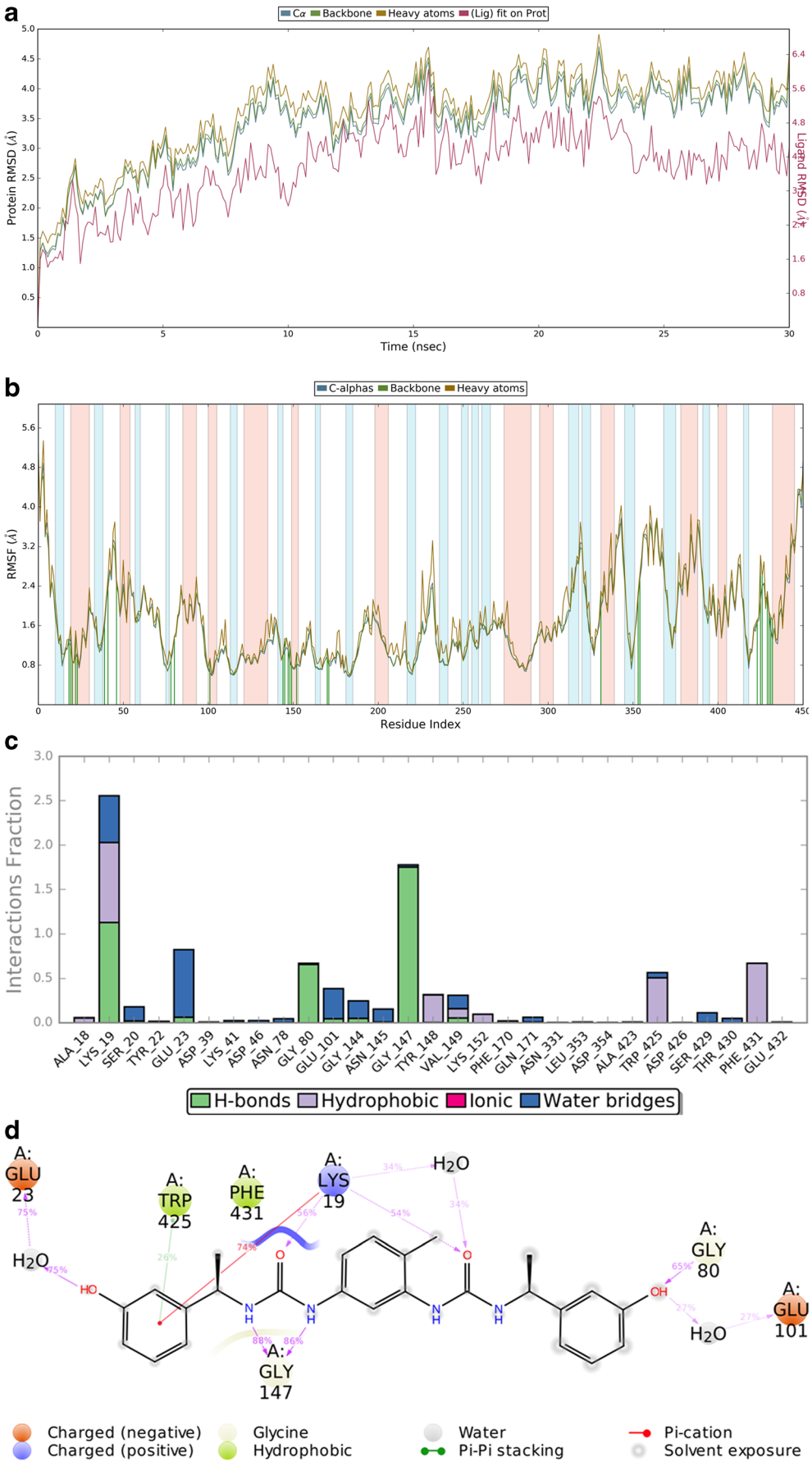

Fig. 3 Represents **a** RMSD (Å) plot of the simulated positions of C-α, backbone, and heavy atoms of modeled *S. aureus* MurD from those in the initial structure. **b** Protein RMSF profile of **H5**/modeled MurD complex during MD simulation. **c** Virtual hit **H5** and modeled MurD protein interaction fraction plot during MD simulation. **d** 2D interaction diagram of **H5** with the catalytic pocket binding residues of modeled MurD protein throughout 30-ns simulation trajectory

S. aureus (MRSA strain 43,300) at high concentrations, while compound **H10** was inactive against all the tested bacterial strains. The lower activity of compound **H5** and inactivity of compound **H10** against the tested bacterial strains is probably due to the failure of these compounds to enter the bacterial cell. Further stability of compound **H5**/*S. aureus* MurD complex was validated by 30-ns molecular dynamics simulation. Hydrogen bonding interactions with Lys19, Glu23, Gly80, and Gly147 as well as π-cation interaction with Lys19 played a crucial role in the stabilization of inhibitor within the catalytic pocket. Hydrophobic interaction was observed to be less significant for the inhibitor binding to *S. aureus* MurD enzyme.

Funding information We would like to thank the Science and Engineering Research Board (SERB), Government of India, for the financial support (No. EMR/2016/002981).

Compliance with ethical standards

Conflict of interest The authors declare that they have no conflict of interest.

Abbreviations *DAP,* 2,6-diaminopimelic acid; *D-Glu,* d-glutamic acid; *MurC,* UDP-N-acetylmuramate:L-Ala ligase; *MRSA,* methicillin-resistant *Staphylococcus aureus*; *MIC,* minimum inhibitory concentration; *MBC,* minimum bactericidal concentration; *MurD,* UDP-N-acetylmuramoyl-L-Ala:D-Glu ligase; *MurE,* UDP-N-acetylmuramoyl-L-Ala-D-Glu:meso-DAP ligase; *MurF,* UDPN-acetylmuramoyl-L-Ala-g-D-Glu-meso-DAP (or L-Lys):D-Ala-D-Ala ligase; *MurNAc,* N-acetylmuramic acid; *UDP,* uridine-5′-diphosphate; *RMSD,* root mean square deviation; *UMA,* uridine-5′-diphosphate-N-acetylmueamoyl-L-alanine; *UMAG,* UDP-N-acetylmuramoyl-L-alanine-D-glutamat

References

1. World Health Organization. Antimicrobial resistance: global report on surveillance. (2014), http://apps.who.int/iris/bitstream/10665/112647/1/WHO_HSE_PED_AIP_2014.2_eng.pdf?ua=1. Accessed 20 Jan 2018
2. Nambiar S, Laessig K, Toerner J, Farley J, Cox E (2014) Antibacterial drug development: challenges, recent developments, and future considerations. Clin Pharmacol Ther 96:147–149
3. Duval X, Delahaye F, Alla F, Tattevin P, Obadia JF, Le Moing V, Doco-Lecompte T, Celard M, Poyart C, Strady C, Chirouze C, Bes M, Cambau E, Iung B, Selton-Suty C, Hoen B (2012) Temporal trends in infective endocarditis in the context of prophylaxis guideline modifications: three successive population-based surveys. J Am Coll Cardiol 59:1968–1976
4. Fedeli U, Schievano E, Buonfrate D, Pellizzer G, Spolaore P (2011) Increasing incidence and mortality of infective endocarditis: a population-based study through a record-linkage system. BMC Infect Dis 11:48
5. Barreteau H, Kovac A, Boniface A, Sova M, Gobec S, Blanot D (2008) Cytoplasmic steps of peptidoglycan biosynthesis. FEMS Microbiol Rev 32:168–207
6. Smith CA (2006) Structure, function and dynamics in the mur family of bacterial cell wall ligases. J Mol Biol 362:640–655
7. Bouhss A, Dementin S, van Heijenoort J, Parquet C, Blanot D (2002) MurC and MurD synthetases of peptidoglycan biosynthesis: borohydride trapping of acylphosphate intermediates. Methods Enzymol 354:189–196
8. Eveland SS, Pompliano DL, Anderson MS (1997) Conditionally lethal Escherichia coli murein mutants contain point defects that map to regions conserved among murein and folyl poly-g-glutamate ligases: identification of a ligase superfamily. Biochem 36:6223–6229
9. Bouhss A, Dementin S, Parquet C, Mengin-Lecreulx D, Bertrand JA, Le Beller D, Dideberg O, van Heijenoort J, Blanot D (1999) Role of the ortholog and paralog amino acid invariants in the active site of the UDP-MurNAc-l-alanine:D-glutamate ligase (MurD). Biochem 38:12240–12247
10. van Heijenoort J (2001) Recent advances in the formation of the bacterial peptidoglycan monomer unit. Nat Prod Rep 18:503–519
11. Skedelj V, Tomasic T, Masic LP, Zega A (2011) ATP-binding site of bacterial enzymes as a target for antibacterial drug design. J Med Chem 54:915–929
12. Walsh AW, Falk PJ, Thanassi J, Discotto L, Pucci MJ, Ho HT (1999) Comparison of the D-glutamate-adding enzymes from selected gram-positive and gram-negative bacteria. J Bacteriol 181:5395–5401
13. El Zoeiby A, Sanschagrin F, Levesque RC (2003) Structure and function of the Mur enzymes: development of novel inhibitors. Mol Microbiol 47:1–12
14. El-Sherbeini M, Geissler WM, Pittman J, Yuan X, Wong KK, Pompliano DL (1998) Cloning and expression of *Staphylococcus aureus* and *Streptococcus pyogenes murD* genes encoding uridine diphosphate *N*-acetylmuramoyl-L-alanine:D-glutamate ligases. Gene 210:117–125
15. Bertrand JA, Auger G, Martin L, Fanchon E, Blanot D, Le Beller D, van Heijenoort J, Dideberg O (1999) Determination of the MurD mechanism through crystallographic analysis of enzyme complexes. J Mol Biol 289:579–590
16. Gordon E, Flouret B, Chantalat L, van Heijenoort J, Mengin-Lecreulx D, Dideberg O (2001) Crystal structure of UDP-N-acetylmuramoyl-L-alanyl-D-glutamate: meso-diaminopimelate ligase from *Escherichia coli*. J Biol Chem 276:10999–11006
17. Yan Y, Munshi S, Leiting B, Anderson MS, Chrzas J, Chen Z (2000) Crystal structure of Escherichia coli UDPMurNAc-tripeptide d-alanyl-d-alanine-adding enzyme (MurF) at 2.3 A resolution. J Mol Biol 304:435–445
18. Perdih A, Kotnik M, Hodoscek M, Solmajer T (2007) Targeted molecular dynamics simulation studies of binding and conformational changes in *E. coli* MurD. Proteins 68:243–254
19. Bouhss A, Mengin-Lecreulx D, Blanot D, van Heijenoort J, Parquet C (1997) Invariant amino acids in the Mur peptide synthetases of bacterial peptidoglycan synthesis and their modification by site-directed mutagenesis in the UDP-MurNAc:L-alanine ligase from *Escherichia coli*. Biochem 36:11556–11563
20. Barreteau H, Sosic I, Turk S, Humljan J, Tomasic T, Zidar N, Herve M, Boniface A, Peterlin-Masic L, Kikelj D, Mengin-Lecreulx D, Gobec S, Blanot D (2012) MurD enzymes from different bacteria: evaluation of inhibitors. Biochem Pharmacol 84:625–632
21. Gegnas LD, Waddell ST, Chabin RM, Reddy S, Wong KK (1998) Inhibitors of the bacterial cell wall biosynthesis enzyme MurD. Bioorg Med Chem Lett 8:1643–1648
22. Gobec S, Urleb U, Auger G, Blanot D (2001) Synthesis and biochemical evaluation of some novel N-acyl phosphono- and phosphinoalanine derivatives as potential inhibitors of the D-glutamic acid-adding enzyme. Die Pharmazie 56:295–297
23. Strancar K, Blanot D, Gobec S (2006) Design, synthesis and structure–activity relationships of new phosphinate inhibitors of MurD. Bioorg Med Chem Lett 16:343–348

24. Auger G, van Heijenoort J, Blanot D (1995) Synthesis of N-Acetylmuramic acid derivatives as potential inhibitors of the D-glutamic acid-adding enzyme. J Prakt Chem 337:351–357
25. Kotnik M, Humljan J, Contreras-Martel C, Oblak M, Kristan K, Hervé M, Blanot D, Urleb U, Gobec S, Dessen A, Solmajer T (2007) Structural and functional characterization of enantiomeric glutamic acid derivatives as potential transition state analogue inhibitors of MurD ligase. J Mol Biol 370:107–115
26. Humljan J, Kotnik M, Contreras-Martel C, Blanot D, Urleb U, Dessen A, Solmajer T, Gobec S (2008) Novel naphthalene-N-sulfonyl-D-glutamic acid derivatives as inhibitors of MurD, a key peptidoglycan biosynthesis enzyme. J Med Chem 51:7486–7494
27. Pratviel-Sosa F, Acher F, Trigalo F, Blanot D, Azerad R, van Heijenoort J (1994) Effect of various analogues of D-glutamic acid on the D-glutamate-adding enzyme from *Escherichia coli*. FEMS Microbiol Lett 115:223–228
28. Perdih A, Bren U, Solmajer T (2009) Binding free energy calculations of N-sulphonyl-glutamic acid inhibitors of MurD ligase. Mol Model 15:983–996
29. Sova M, Kovac A, Turk S, Hrast M, Blanot D, Gobec S (2009) Phosphorylated hydroxyethylamines as novel inhibitors of the bacterial cell wall biosynthesis enzymes MurC to MurF. Bioorg Chem 37:217–222
30. Zidar N, Tomasic T, Sink R, Rupnik V, Kovac A, Turk S, Patin D, Blanot D, Contreras Martel C, Dessen A, Müller Premru M, Zega A, Gobec S, Peterlin Masic L, Kikelj D (2010) Discovery of novel 5-benzylidenerhodanine and 5-benzylidenethiazolidine-2,4-dione inhibitors of MurD ligase. J Med Chem 53:6584–6594
31. Zidar N, Tomasic T, Sink R, Kovac A, Patin D, Blanot D, Contreras-Martel C, Dessen A, Premru MM, Zega A, Gobec S, Masic LP, Kikelj D (2011) New 5-benzylidenethiazolidin-4-one inhibitors of bacterial MurD ligase: design, synthesis, crystal structures, and biological evaluation. Eur J Med Chem 46:5512–5523
32. Sosic I, Barreteau H, Simcic M, Sink R, Cesar J, Zega A, Grdadolnik SG, Contreras-Martel C, Dessen A, Amoroso A, Joris B, Blanot D, Gobec S (2011) Second-generation sulfonamide inhibitors of D-glutamic acid-adding enzyme: activity optimisation with conformationally rigid analogues of D-glutamic acid. Eur J Med Chem 46:2880–2894
33. Perdih A, Hrast M, Barreteau H, Gobec S, Wolber G, Solmajer T (2014) Benzene-1,3-dicarboxylic acid 2,5-dimethylpyrrole derivatives as multiple inhibitors of bacterial Mur ligases (MurC-MurF). Bioorg Med Chem 22:4124–4134
34. Perdih A, Kovac A, Wolber G, Blanot D, Gobec S, Solmajer T (2009) Discovery of novel benzene 1,3-dicarboxylic acid inhibitors of bacterial MurD and MurE ligases by structure-based virtual screening approach. Bioorg Med Chem Lett 19:2668–2673
35. Turk S, Kovac A, Boniface A, Bostock JM, Chopra I, Blanot D, Gobec S (2009) Discovery of new inhibitors of the bacterial peptidoglycan biosynthesis enzymes MurD and MurF by structure-based virtual screening. Bioorg Med Chem 17:1884–1889
36. Kotnik M, Anderluh PS, Prezelj A (2007) Development of novel inhibitors targeting intracellular steps of peptidoglycan biosynthesis. Curr Pharm Des 13:2283–2309
37. Tomasic T, Zidar N, Sink R, Kovac A, Blanot D, Contreras-Martel C, Dessen A, Muller-Premru M, Zega A, Gobec S, Kikelj D, Masic LP (2011) Structure-based design of a new series of D-glutamic acid based inhibitors of bacterial UDP-N-acetylmuramoyl-L-alanine:D-glutamate ligase (MurD). J Med Chem 54:4600–4610
38. Tomasic T, Sink R, Zidar N, Fic A, Contreras-Martel C, Dessen A, Patin D, Blanot D, Muller-Premru M, Gobec S, Zega A, Kikelj D, Masic LP (2012) Dual inhibitor of MurD and MurE ligases from *Escherichia coli* and *Staphylococcus aureus*. ACS Med Chem Lett 3:626–630
39. Azam MA, Jupudi S, Saha N, Paul RK (2018) Combining molecular docking and molecular dynamics studies for modelling Staphylococcus aureus MurD inhibitory activity. SAR QSAR Environ Res 30:1–20
40. Friesner RA, Murphy RB, Repasky MP, Frye LL, Greenwood JR, Halgren TA, Sanschagrin PC, Mainz DT (2006) Extra precision glide: docking and scoring incorporating a model of hydrophobic enclosure for protein-ligand complexes. J Med Chem 49:6177–6196
41. Jacobson MP, Pincus DL, Rapp CS, Day TJ, Honig B, Shaw DE, Friesner RA (2004) A hierarchical approach to all-atom protein loop prediction. Proteins: Struct Funct Bioinf 55:351–367
42. Li J, Abel R, Zhu K, Cao Y, Zhao S, Friesner RA (2011) The VSGB 2.0 model: a next generation energy model for high resolution protein structure modelling. Proteins 79:2794–2812
43. Guo Z, Mohanty U, Noehre J, Sawyer TK, Sherman W, Krilov G (2010) Probing the α-helical structural stability of stapled p53 peptides: molecular dynamics simulations and analysis. Chem Biol Drug Des 75:348–359
44. Harder E, Damm W, Maple J, Wu C, Reboul M, Xiang JY, Wang L, Lupyan D, Dahlgren MK, Knight JL, Kaus JW, Cerutti DS, Krilov G, Jorgensen WL, Abel R, Friesner RA (2016) OPLS3: a force field providing broad coverage of drug-like small molecules and proteins. J Chem Theory Comput 12:281–296
45. Jorgensen WJ, Madura JD (1985) Temperature and size dependence for Monte Carlo simulations of TIP4P water. Mol Phys 56:1381–1392
46. Lawrence CP, Skinner JL (2003) Flexible TIP4P model for molecular dynamics simulation of liquid water. Chem Phys Lett 372:842–847
47. Essmann U, Perera L, Berkowit ML, Darden T, Lee H, Pedersen LG (1995) A smooth particle mesh Ewald method. J Chem Phys 103:8577–8593
48. Martyna GJ, Klein ML, Tuckerman M (1992) Nose-Hoover chains: the canonical ensemble via continuous dynamics. J Chem Phys 97:2635–2643
49. Martyna GJ, Tobias DJ, Klein ML (1994) Constant-pressure molecular dynamics algorithms. J Chem Phys 101:4177–4189
50. Auger G, Martin L, Bertrand J, Ferrari P, Fanchon E, Vaganay S, Petillot Y, van Heijenoort J, Blanot D, Dideberg O (1998) Large-scale preparation, purification, and crystallization of UDP-N-acetylmuramoyl-L-alanine: D-glutamate ligase from *Escherichia coli*. Prot Express Purif 13:23–29
51. Lanzetta PA, Alvarez LJ, Reinach PS, Candia OA (1979) An improved assay for nanomole amounts of inorganic phosphate. Anal Biochem 100:95–97
52. Clinical and Laboratory Standard Institute (CLSI) (2007) Methods for dilution antibacterial susceptibility test for Bacteria that grow aerobically, 7th ed. Approved Standard (MA7-A7); Clinical and Laboratory Standard Institute: Wayne. 27:133
53. Tomasic T, Kovac A, Simcic M, Blanot D, Grdadolnik SG, Gobec S, Kikelj D, Peterlin Masic L (2011) Novel 2-thioxothiazolidin-4-one inhibitors of bacterial MurD ligase targeting D-Glu- and diphosphate-binding sites. Eur J Med Chem 46:3964–3975

Publisher's note Springer Nature remains neutral with regard to jurisdictional claims in published maps and institutional affiliations.